

4 **Neuromodulatory changes in short-term synaptic dynamics**
5 **may be mediated by two distinct mechanisms of presynaptic**
6 **calcium entry**7 **Myongkeun Oh · Shunbing Zhao · Victor Matveev ·**
8 **Farzan Nadim**9 Received: 6 October 2011 / Revised: 9 May 2012 / Accepted: 23 May 2012
10 © Springer Science+Business Media, LLC 2012

11

12 **Abstract** Although synaptic output is known to be modu-
13 lated by changes in presynaptic calcium channels, additional
14 pathways for calcium entry into the presynaptic terminal,
15 such as non-selective channels, could contribute to modula-
16 tion of short term synaptic dynamics. We address this issue
17 using computational modeling. The neuropeptide proctolin
18 modulates the inhibitory synapse from the lateral pyloric
19 (LP) to the pyloric dilator (PD) neuron, two slow-wave
20 bursting neurons in the pyloric network of the crab *Cancer*
21 *borealis*. Proctolin enhances the strength of this synapse and
22 also changes its dynamics. Whereas in control saline the
23 synapse shows depression independent of the amplitude of
24 the presynaptic LP signal, in proctolin, with high-amplitude
25 presynaptic LP stimulation the synapse remains depressing
26 while low-amplitude stimulation causes facilitation. We use
27 simple calcium-dependent release models to explore two
28 alternative mechanisms underlying these modulatory
29 effects. In the first model, proctolin directly targets calcium

channels by changing their activation kinetics which results 30
in gradual accumulation of calcium with low-amplitude 31
presynaptic stimulation, leading to facilitation. The second 32
model uses the fact that proctolin is known to activate a non- 33
specific cation current I_{MI} . In this model, we assume that the 34
MI channels have some permeability to calcium, modeled to 35
be a result of slow conformation change after binding cal- 36
cium. This generates a gradual increase in calcium influx 37
into the presynaptic terminals through the modulatory chan- 38
nel similar to that described in the first model. Each of these 39
models can explain the modulation of the synapse by pro- 40
ctolin but with different consequences for network activity. 41

Keywords Neuromodulation · Proctolin · Short-term 42
synaptic dynamics · Pyloric network 43

44 **1 Introduction**

Short-term synaptic dynamics such as facilitation and de- 45
pression are observed in most synapses (Mamiya et al. 2003; 46
Pan and Zucker 2009; Zucker and Regehr 2002). Although 47
the functional significance of these forms of synaptic plas- 48
ticity in oscillatory networks is still mostly unknown, sev- 49
eral studies have proposed a variety of roles for synaptic 50
dynamics that is important for the proper function of these 51
networks (Abbott et al. 1997; Chance et al. 1998; Dittman et 52
al. 2000; Galarreta and Hestrin 1998; K. M. MacLeod et al. 53
2007; Mamiya and Nadim 2005; Manor et al. 2003; Nadim 54
et al. 2003; Reyes et al. 1998; Rose and Fortune 1999; M. V. 55
Tsodyks and Markram 1997). Most synapses are also sub- 56
ject to neuromodulation that changes their strength and 57
short-term dynamics (Barriere et al. 2008; Kreitzer and 58
Regehr 2000). The neuromodulators that change synaptic 59
release often do so by targeting presynaptic voltage-gated 60
calcium channels (Wu and Saggau 1997; Bieda and 61

Communicated by **Action Editor: C. Linster**

M. Oh · V. Matveev · F. Nadim
Department of Mathematical Sciences,
New Jersey Institute
of Technology,
Newark, NJ 07102, USA

M. Oh
e-mail: mo42@njit.edu

V. Matveev
e-mail: matveev@njit.edu

S. Zhao · F. Nadim (✉)
Department of Biological Sciences, Rutgers University,
195 University Ave.,
Newark, NJ 07102, USA
e-mail: farzan@njit.edu

S. Zhao
e-mail: shunbing@gmail.com

Q5

62 Copenhagen 2004; Wang et al. 2006; Zucker and Regehr
 63 2002). Neuromodulators also target other types of ion chan-
 64 nels that may be permeable to calcium but not known to be
 65 involved in synaptic transmission. It is possible that calcium
 66 entry through such channels may act as a modulator of
 67 synaptic dynamics (Verhoog and Mansvelder 2011;
 68 Bardoni et al. 2004; Berretta and Jones 1996). Here we
 69 use a computational model to examine the mechanisms by
 70 which neuromodulators could affect synaptic strength and
 71 dynamics through direct effects on presynaptic voltage gated
 72 calcium channels and through indirect effects mediated by
 73 calcium entry through non-specific cation current channels.

74 The oscillatory pyloric network of the crab stomatogas-
 75 tric nervous system is an extensively studied system for the
 76 effects of neuromodulators (Marder and Bucher 2007).
 77 Previous studies of the pyloric network have explored the
 78 actions of neuromodulators on ionic currents (Johnson et al.
 79 2003), synaptic strength (Ayali et al. 1998; Thirumalai et al.
 80 2006) and, more recently, short-term synaptic dynamics
 81 (Johnson et al. 2011; Johnson et al. 2005; Zhao et al.
 82 2011). The Zhao et al. (2011) study examined the effect of
 83 the endogenous neuropeptide proctolin on the strength and
 84 short-term dynamics of the inhibitory synapse from the LP
 85 to the PD neuron in the pyloric network. This synapse is the
 86 sole chemical feedback from the pyloric follower neurons to
 87 its pacemaker group and its dynamics are potentially impor-
 88 tant in shaping the network output. The LP to PD synapse is
 89 dominated by a strong graded component whose strength is
 90 enhanced by proctolin. The short-term dynamics of this
 91 component are also modified by proctolin in an unusual
 92 manner: the synapse shows short-term depression in control
 93 saline whereas, in the presence of proctolin, low-amplitude
 94 (<25 mV) presynaptic stimulation causes facilitation, while
 95 high-amplitude (>25 mV) stimulation causes depression.
 96 Although the mechanisms underlying these synaptic modifi-
 97 cations by proctolin are not known, the switch from depression
 98 to facilitation is correlated with slowly accumulating Ca^{2+}
 99 entry in the presynaptic cell in the presence of proctolin,
 100 suggesting a presynaptic mechanism (Zhao et al. 2011).

101 We investigate possible mechanisms underlying the mod-
 102 ulation of the strength and short-term dynamics of the LP to
 103 PD synapse by proctolin by considering two simple mech-
 104 anistic models that explain the observed effects of proctolin.
 105 In the first model, which is based on a previous more
 106 detailed model (Zhou et al. 2007), we examine the possibil-
 107 ity that proctolin targets the presynaptic voltage-dependent
 108 calcium currents (I_{Ca}), consistent with the observed increase
 109 in Ca^{2+} influx from pulse to pulse (see Fig. 1). Calcium
 110 currents are a common target through which modulators can
 111 regulate transmitter release (Fossier et al. 1999; Hige et al.
 112 2006; Johnson et al. 2003; Wu and Saggau 1997). In this
 113 model, proctolin modifies the activation kinetics of I_{Ca} in
 114 the LP neuron which, in turn, results in different levels of

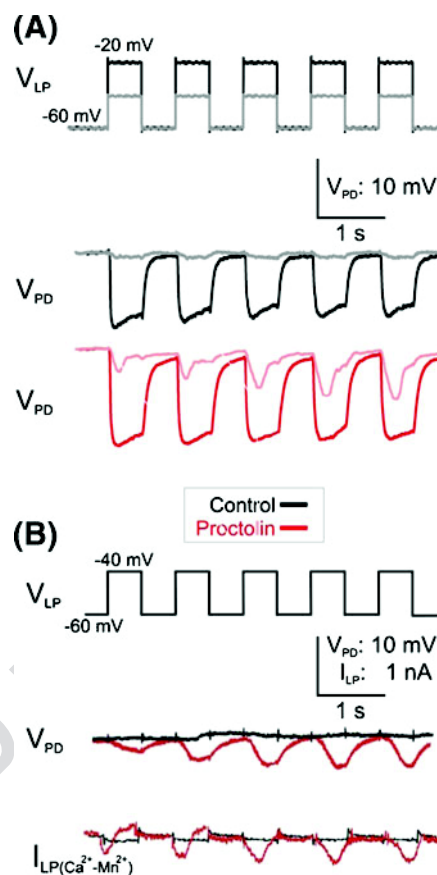


Fig. 1 Proctolin modulates the short-term dynamics of the LP to PD inhibitory synapse in response to presynaptic depolarization pulses of different amplitude. (a) LP neuron was voltage-clamped at -60 mV and stimulated with a series of five square pulses of 40 mV (V_{LP} : black trace) or 20 mV (V_{LP} : gray trace) amplitudes in control saline and in 10^{-6} M proctolin and the synaptic potentials were recorded in the PD neuron. In control saline the LP to PD synapse was depressing. In proctolin, in response to 20 mV presynaptic pulses, the synapse showed facilitation (pink) but it remained depressing (red) in response to the 40 mV pulses. (b) The proctolin-induced facilitation of the LP to PD synapse in response to low amplitude 20 mV presynaptic pulses is associated with the activation of Ca^{2+} -like inward current $\Delta I_{LP} = I_{LP}(Ca^{2+}) - I_{LP}(Mn^{2+})$ (Zhao et al. 2011). The amplitude of the current ΔI_{LP} exhibits no change in control (black) and increases in proctolin (red) with each pulse

115 calcium entry in this neuron depending on the amplitude and
 116 timing of the LP neuron membrane potential. The distinct
 117 levels of calcium concentration in the LP neuron, in turn,
 118 result in different levels of synaptic release.

119 A second related model takes into account the fact that
 120 proctolin activates a voltage-gated modulatory inward cur-
 121 rent, I_{MI} (Golowasch and Marder 1992; Swensen and
 122 Marder 2000). I_{MI} is a nonspecific cation current, permeable
 123 to Na^{+} and K^{+} , whose gating properties were shown by
 124 Golowasch and Marder (1992) to be strongly affected by
 125 extracellular Ca^{2+} , suggestive of an external pore block by
 126 Ca^{2+} ions, much like the Mg^{2+} block in NMDA-receptor
 127 channels. In this model, we assume that the Ca^{2+} block of

128 the I_{MI} channels is not total and the channels are partially
 129 permeable to Ca^{2+} . In the presence of proctolin, the MI
 130 channels are activated, thus providing an additional source
 131 of Ca^{2+} ions in the presynaptic LP neuron which, together
 132 with the Ca^{2+} entry through voltage-gated Ca^{2+} -channels,
 133 accounts for the modulation of synaptic release. The modu-
 134 lation of the short-term synaptic plasticity in this model
 135 depends on the slow kinetics of Ca^{2+} influx through the
 136 MI channels.

137 Because of the limited number of elements in our models,
 138 we can use an optimization algorithm to find the parameter
 139 sets that best fit the experimental data. The optimization
 140 algorithm produces a number of parameter sets that are
 141 consistent with the observed neuromodulatory effects of
 142 proctolin on this synapse. Analysis of these data sets can
 143 reveal the features of the model that are most critical for
 144 explaining the experimental data, and the correlations be-
 145 tween parameter values can be used to uncover the inter-
 146 dependence among different model elements. Interestingly,
 147 each of the two proposed models of proctolin action can
 148 explain the modulation of the LP to PD synapse by proctol-
 149 in, but the two models point to different targets of action by
 150 this neuromodulator.

151 **2 Methods**

152 Each model consists of a set of differential equations
 153 that describe the ionic currents I_{Ca} or I_{MI} and the
 154 intracellular calcium concentration $[Ca^{2+}]_i$ in the presyn-
 155 aptic LP neuron, as well as a passive model that cap-
 156 tures the synaptic potential in the postsynaptic PD
 157 neuron. We make no assumptions on the compartmen-
 158 talization of $[Ca^{2+}]_i$ and therefore all spatial distribution
 159 of Ca^{2+} is ignored. We have measured synaptic poten-
 160 tials in the PD neuron by voltage clamping the presyn-
 161 aptic LP neuron after blocking all neuronal activity and
 162 applying a train of voltage pulses. Therefore, the only
 163 ionic currents considered in the presynaptic LP neuron
 164 are the calcium current I_{Ca} (present in both models) and
 165 the modulator-activated inward current I_{MI} (present only
 166 in model II). We assume that the calcium current in the
 167 LP neuron I_{Ca} has only one component involving both
 168 activation and inactivation processes

Q6
$$I_{Ca} = \bar{g}_{Ca} m^2 h (V - V_{Ca}) \quad (1)$$

169 where $V_{Ca}=100mV$ is the reversal potential and \bar{g}_{Ca} is
 171 the maximum conductance of I_{Ca} . The activation (m)
 172 and inactivation (h) variables are given by

$$\frac{dx}{dt} = \frac{x_{\infty} - x}{\tau_x}, x = m, h \quad (2)$$

where 173

$$m_{\infty} = \frac{1}{1 + \exp\left(-\frac{V+V_m}{S_m}\right)} \quad (3)$$

is the steady-state activation and 176

$$h_{\infty} = \frac{1}{1 + \exp\left(-\frac{V+V_h}{S_h}\right)}$$

is the steady-state inactivation. The time constant of activation 178
 (τ_m) and inactivation (τ_h) are fixed in both cases and produce 179
 sufficient slow recovery of calcium channels from inactivation 180
 for all voltage levels. This slow recovery generates a gradual 181
 decrease in Ca^{2+} current from pulse to pulse. This is the main 182
 mechanism of synaptic depression of the LP to PD synapse in 183
 both models. Experimental observations suggest that I_{Ca} in the 184
 LP neuron consists of two components, a transient and a 185
 sustained one. Because of the slow time constant for inactiva- 186
 tion, the current expression in Eq. (1) provides a simple model 187
 of a composition of these two components. 188

The calcium concentration in the presynaptic LP neuron 189
 is described by 190

$$\frac{d[Ca^{2+}]_i}{dt} = -\frac{[Ca^{2+}]_i}{\tau_{Ca}} - \lambda I_{Ca} \quad (4)$$

where the time constant of calcium (τ_{Ca}) is kept at a constant 192
 value. The last term in Eq. (4) represents the Ca^{2+} influx and 193
 $\lambda = \frac{1}{2FV} = 0.1\mu M/(nAms)$, where F is Faraday's constant 194
 and V is the volume. In model II, Eq. (4) has an additional 195
 term corresponding to the influx through the modulatory 196
 channel (see Eq. (11)). 197

The synaptic current model assumes the standard fourth- 198
 order Ca^{2+} cooperativity of neurotransmitter release 199
 (Schneppenburger and Neher 2005): 200

$$g_{syn} = \bar{g}_{syn} \frac{K_{Ca}^4 [Ca^{2+}]_i^4}{K_{Ca}^4 + [Ca^{2+}]_i^4} \quad (5)$$

where \bar{g}_{syn} is the maximal synaptic conductance and K_{Ca} is 202
 the calcium affinity of neurotransmitter release. 203

The inhibitory postsynaptic potential (IPSP) in the PD 204
 neuron is given by 205

$$C \frac{dV}{dt} = -g_{syn}(V - V_{syn}) - g_m(V - V_{rest}) \quad (6)$$

where $C=1nF$ is the membrane capacitance, $V_{syn}=-80mV$ is 206
 the synaptic reversal potential, $V_{rest}=-60mV$ is the resting 208
 potential of postsynaptic membrane which is a holding 209

210 potential using voltage-clamp in experiment, and g_m is the
 211 intrinsic membrane conductance. These values lie in ranges
 212 consistent with experimental data (Buchholtz et al. 1992;
 213 Golowasch and Marder 1992; Swensen and Marder 2001).

214 In the optimization algorithm, all model parameters (with
 215 the exception of ion reversal potentials, membrane capaci-
 216 tance C and the constant λ in Eq. (4)) were considered to be
 217 free variables and their values were determined by optimiz-
 218 ing the fit between a single experimentally-observed and the
 219 model-simulated potential of the PD neuron. At each step of
 220 the optimization algorithm, corresponding to a particular set
 221 of parameter values, the time course of the PD voltage was
 222 computed both in the control condition and in the presence
 223 of proctolin, for two values of presynaptic stimulation ampli-
 224 tude (20 mV and 40 mV). The numerical solution of
 225 differential equations describing model I or model II was
 226 performed using MATLAB's built-in ode15s solver for stiff
 227 systems (MathWorks, Inc.). The optimized objective func-
 228 tion equals the time integral of the absolute difference be-
 229 tween the observed and the simulated PD voltage time
 230 courses, with an arbitrary scaling freedom between the two
 231 sets of time traces. Deviations corresponding to the four
 232 cases (two amplitudes of presynaptic stimulation in control
 233 and in the presence of proctolin) were all summed together,
 234 resulting in a single cost function. Only a single free scaling
 235 parameter was allowed for the set of all four time traces. An
 236 additional term describing the deviation between the

237 simulated and the observed degree of short-term synaptic
 238 plasticity was added to the objective function, to ensure that
 239 optimization achieves facilitation for small amplitude stim-
 240 ulation in proctolin, and short-term depression for high-
 241 amplitude stimulation. To ensure sufficient sampling of
 242 parameter value ranges, parameter optimization was preced-
 243 ed by a random search through a large volume of the
 244 parameter space, and sufficiently small objective function
 245 values obtained during such random searches were then
 246 used as starting points of subsequent parameter optimiza-
 247 tion. Several hundred random parameter combinations were
 248 typically probed before starting each parameter optimization
 249 run. Only those optimized parameter sets that passed a
 250 goodness-of-fit threshold were included for later analysis.

251 The unconstrained nonlinear minimization of the objec-
 252 tive function (total deviation function) described above is
 253 performed using MATLAB's built-in *fminsearch* routine
 254 (MathWorks, Inc.), which implements derivative-free
 255 Nelder-Mead Simplex Method (Lagarias et al. 1998).

256 In model I, the optimization is performed over the fol-
 257 lowing 16 model parameters (see Results, and Fig. 2):

$$K_{Ca}, \bar{g}_{syn}, \bar{g}_{Ca}, g_m, \tau_h, \tau_{Ca}, \tau_m^c, V_h, S_h, V_m, S_m, V_m^p, S_m^p, A_\tau^p, V_\tau^p, S_\tau^p$$

258 In model II, there are 15 optimized parameters (see
 259 Results and Fig. 5):

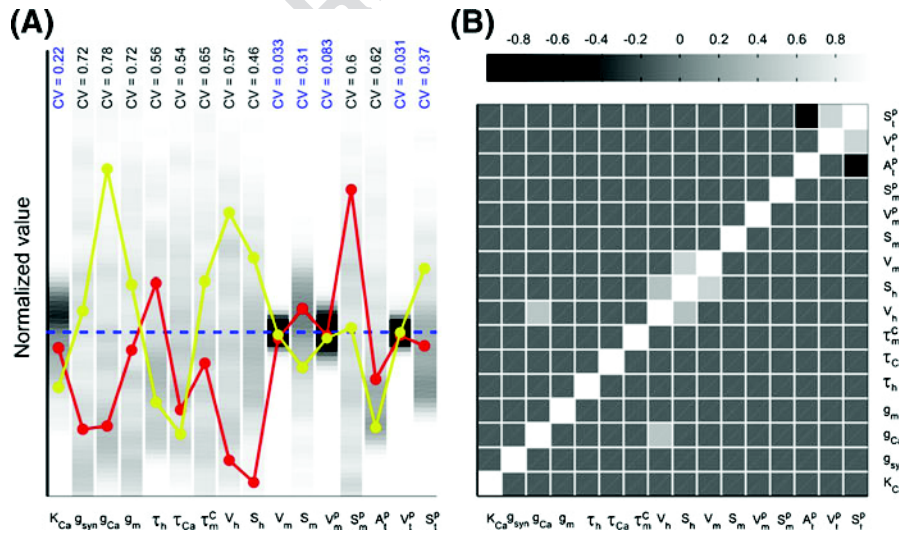


Fig. 2 Optimized parameter sets showing the changes in activation kinetics of presynaptic Ca^{2+} channels in model I. A total of 256 randomly-seeded parameter sets were optimized for model I to fit the experimental recording of the synaptic outputs in control and proctolin for two different presynaptic voltage amplitudes (see Methods). (a) The distribution of parameter values for each of the 16 parameters in model I is indicated in grayscale, with darker tones representing greater distribution density. The value of each parameter was normalized to the mean value of its distribution (dashed blue line) for comparison; these mean values are: $K_{Ca} = 1.3\mu M$, $\bar{g}_{syn} = 14.1nS/\mu M^4$, $\bar{g}_{Ca} = 1.8nS$, $g_m =$

$0.46\mu S$, $\tau_h = 1.6s$, $\tau_{Ca} = 33.6ms$, $\tau_m^c = 39.7ms$, $V_h = 78.5mV$, $S_h = 41mV$, $V_m = 42mV$, $S_m = 8.7mV$, $V_m^p = 50mV$, $S_m^p = 2.8mV$, $A_\tau^p = 2.0s$, $V_\tau^p = 50.5mV$, $S_\tau^p = 5.9mV$ Two parameter sets are also shown for comparison (red and yellow), demonstrating that good fits to the data did not require a consistent relationship among all parameters. Six out of 16 parameters were relatively tightly constrained by the optimization technique (coefficient of variation < 0.4 shown in blue). (b) Pair-wise correlations among the best-fit parameters indicate that few parameter pairs showed any significant ($R > 0.5$) co-variation. See Results for additional description

$$K_{Ca}, \bar{g}_{syn}, \bar{g}_{Ca}, g_m, g_{MI}, \tau_h, \tau_{Ca}, \tau_m, V_h, S_h, V_m, S_m, V^+, S^+, k^-$$

262

263 **3 Results**

264 3.1 Neuromodulation of the LP to PD synapse

265 The LP to PD synapse is known to display short-term
 266 depression in the absence of proctolin (Manor et al. 1997).
 267 To characterize short-term plasticity of the LP to PD syn-
 268 apse, we injected a train of high- and low-amplitude (V_{LP} in
 269 Fig. 1(a)) into the voltage clamped LP neuron and recorded
 270 the postsynaptic potential in the PD neuron (V_{PD} in
 271 Fig. 1(a)). The IPSP recorded in the PD neuron showed
 272 depression with high-amplitude presynaptic pulses and little
 273 response with low-amplitude pulses (Fig. 1(a) Control).
 274 (The low-amplitude response in control is often small or
 275 shows some depression (Zhao et al. 2011).) In contrast, the
 276 IPSP in proctolin showed depression with high-amplitude
 277 pulses but facilitation with low-amplitude pulses (Fig. 1(a)
 278 Proctolin).

279 As we have reported previously, this change in the short-
 280 term synaptic dynamics in the presence of proctolin is
 281 independent of the waveform shape used and is also present
 282 when the presynaptic neuron is voltage clamped with real-
 283 istic bursting waveforms (Zhao et al. 2011). Here, we will
 284 focus primarily on the response to a train of depolarizing
 285 square pulses to simplify the description of the kinetics that
 286 may be involved in producing short-term depression or
 287 facilitation.

288 To unmask the underlying cause for facilitation, the
 289 experiments with low-amplitude pulses were performed in
 290 saline containing normal levels of Ca^{2+} or after substituting
 291 the Ca^{2+} with Mn^{2+} (and therefore blocking synaptic trans-
 292 mission), in both control and in 10^{-6} M proctolin (Fig. 1(b)).
 293 In all conditions, we made simultaneous measurements of
 294 the presynaptic current (I_{LP}) and the postsynaptic potential.
 295 The difference between the presynaptic currents measured
 296 in normal saline and in Mn^{2+} was considered a putative Ca^{2+}
 297 current ($\Delta I_{LP} = I_{LP(Ca^{2+})} - I_{LP(Mn^{2+})}$ in Fig. 1(b)). In the
 298 example shown, in control saline there was little synaptic
 299 response and no apparent synaptic plasticity was observed
 300 (V_{PD} , black trace in Fig. 1(b)). In contrast, the synaptic
 301 response showed facilitation in proctolin (with normal
 302 Ca^{2+} ; V_{PD} , red curve in Fig. 1(b)). The putative calcium
 303 current was small in control conditions and its amplitude
 304 showed no variation with each subsequent pulse (ΔI_{LP} black
 305 trace in Fig. 1(b)). However, in the presence of proctolin, this
 306 current increased in amplitude with each subsequent pulse,
 307 indicating accumulation of Ca^{2+} currents (ΔI_{LP} red trace in
 308 Fig. 1). When the average amplitudes of the presynaptic

inward current ΔI_{LP} and the IPSPs are compared, there is a
 positive correlation between the presynaptic inward current
 and the postsynaptic potentials (Zhao et al. 2011).

The data shown indicated that facilitation is likely caused
 primarily by an increase in Ca^{2+} current from pulse to pulse,
 rather than slow clearance of free or bound residual $[Ca^{2+}]_i$
 (Zucker and Regehr 2002). Increase in Ca^{2+} influx has been
 shown to underlie short-term facilitation in other synapses
 as well (Bertram et al. 2003; Xu et al. 2007). Thus, any
 minimal model of proctolin effects on synaptic dynamics
 should involve a mechanism of calcium influx modulation
 by proctolin. Here we propose two possible mathematical
 models based on the kinetics of voltage-gated Ca^{2+} currents
 in the presynaptic LP neuron to explore the mechanisms
 underlying the effects of proctolin described above.

3.2 Model I: Ca^{2+} -channel model

In model I, we assumed that proctolin targets and modifies the
 activation kinetics and activation time constant of presynaptic
 Ca^{2+} channels. Such a change of kinetics and time constant
 constitute a minimal assumption allowing the model to repro-
 duce experimentally observed voltage-dependence of the shift
 from depression to facilitation by proctolin.

The activation time constant of I_{Ca} in control conditions
 was set to a constant value τ_m^c . This time constant was
 allowed to be modulated by proctolin under the functional
 constraint:

$$\tau_m^p(V) = \frac{A_\tau^p}{\cosh\left(\frac{V+V_\tau^p}{S_\tau^p}\right)} \tag{7}$$

Parameters A_τ^p , V_τ^p and S_τ^p (determined by data fit
 optimization) yield activation which is slow at low voltages
 but fast at high voltages. Further, we assumed that the steady-
 state activation parameters V_m and S_m for m_∞ given by Eq. (3)
 is altered by proctolin; we denote the corresponding values V_m^p
 and S_m^p (see Fig. 2 (a)).

All model parameters were determined using an optimi-
 zation algorithm to fit the observed time courses of postsyn-
 aptic potentials in both control and proctolin conditions and
 with presynaptic amplitudes of 20 mV and 40 mV. A total of
 256 randomly-seeded parameter sets were optimized (see
 Methods) and the overall range of parameter distributions
 obtained for the fits is shown in Fig. 2. About a thousand
 other randomly seeded optimized parameter sets that did not
 pass our goodness of fit threshold were excluded from our
 analysis.

Within the best fits, the majority of the 16 optimized
 model parameters had values with a wide distribution, as
 seen in the coefficient of variation of the normalized param-
 eter values ($CV \geq 0.4$; Fig. 2(a)). The high variability of the

357 conductance parameters in particular is at least in part
 358 explained by the scaling freedom between model and ex-
 359 perimental data (see Methods). However, some parameters,
 360 such as the midpoint and slope (only in control) of the Ca^{++}
 361 current activation curve and the parameters determining its
 362 time constant in proctolin were relatively constrained ($CV <$
 363 0.4). Another constrained parameter was K_{Ca} , the calcium
 364 affinity of neurotransmitter release.

365 As seen in the two examples shown in Fig. 2(a), there
 366 was no global relationship among parameter sets that pro-
 367 vided best fit values in this model. We therefore examined
 368 whether there are two-parameter correlations among these
 369 parameters. Few parameter pairs showed strong positive or
 370 negative pair-wise correlations and those that did were
 371 mostly restricted to the parameters of the Ca^{++} current
 372 activation curve and time constant (Fig 2(b)).

373 Figure 3 demonstrates the effects of proctolin in model I
 374 for one optimized parameter set (red parameter set in Fig. 2
 375 (a)) in response to two different voltage levels in the pre-
 376 synaptic LP neuron, both in control (left panels) and in
 377 proctolin (right panels). For any presynaptic pulse ampli-
 378 tude, the model shows an increase in Ca^{2+} influx through the
 379 Ca^{2+} channels, leading to greater IPSP amplitude in PD
 380 neuron in proctolin than in control due to the modification
 381 of steady-state activation of Ca^{2+} channels by proctolin
 382 (Fig. 3 (e) and (f)).

383 The change in the activation curve and kinetics results in
 384 a significantly greater IPSP in the PD neuron due to the
 385 gradual increase in free residual Ca^{2+} concentration in the
 386 presynaptic terminal for low presynaptic voltage pulses.
 387 This, in turn, results in a shift of the synaptic activation
 388 curve to lower voltages, consistent with the predictions from
 389 experimental data (Zhao et al. 2011).

390 In this model, proctolin application resulted in much
 391 slower activation of Ca^{2+} channels at low voltages as com-
 392 pared to control, leading to synaptic facilitation due to a
 393 slow accumulation of I_{Ca} . For the high-amplitude (40 mV)
 394 pulses, synaptic depression is present both in control and in
 395 proctolin, since the time constant of activation at high vol-
 396 tage is close to the value in the control condition.

397 3.3 Model II: Modulatory channel model

398 In this model, we explored the alternative hypothesis that
 399 Ca^{2+} influx through MI channels can sufficiently describe
 400 the effects of proctolin on synaptic strength and dynamics
 401 without any direct modulation of the Ca^{2+} current. Previous
 402 experimental studies have suggested that MI channels are
 403 blocked by Ca^{2+} at low presynaptic voltages. The removal
 404 of Ca^{2+} from the extracellular medium results in a linear $I-V$
 405 relationship for I_{MI} , much like the effect of removing Mg^{2+}
 406 on NMDA receptor channels (Golowasch and Marder
 407 1992). Therefore, it is conceivable that modulatory channel

binding with Ca^{2+} would induce a slow conformation 408
 change of this channel that leads to a greater calcium 409
 influx. This would lead to a change in Ca^{2+} permeability of this 410
 channel when Ca^{2+} block is removed by depolarization. 411
 This putative mechanism is analogous to Mg^{2+} influx 412
 through NMDA channel which occurs even though the 413
 channels are blocked by Mg^{2+} (Stout et al. 1996). We 414
 propose a conformational change in the MI channels based 415
 on the following state diagram: 416



Our hypothesis for MI channel gating is inspired in part 418
 by the mechanism of Ca^{2+} -dependent inactivation of L-type 419
 Ca^{2+} channels (Babich et al. 2007; Yue et al. 1990; Olcese 420
 2007). Namely, we assume in our model that channel state 421
 C^0 has the highest affinity for Ca^{2+} , so its pore is completely 422
 blocked by Ca^{2+} , leading to zero cation permeability. 423
 Channel state C^1 has lower but significant Ca^{2+} affinity, 424
 allowing only Ca^{2+} ions to pass through upon their binding 425
 to the channel pore selectivity site. Finally, state O has very 426
 low Ca^{2+} affinity, allowing unrestricted flow of Na^+ and K^+ 427
 as well as Ca^{2+} through this channel (see Fig. 4(a)). 428

429 Because both states C^1 and O are assumed to have non-
 zero permeability to Ca^{2+} , and because only Ca^{2+} currents
 are responsible for synaptic response, for simplicity we
 combined these two states into a single open state x when
 calculating the effect of this channel on Ca^{2+} entry, with the
 transition between the open and closed states governed by a
 constant backward rate and a voltage-dependent forward
 rate given by: 437

$$k^+(V) = \frac{1}{1 + \exp\left(-\frac{V+V^+}{S^+}\right)} ms^{-1}$$

438 The time constant of the MI current activation is given by
 the reciprocal of the sum of the forward and backward rates. 439
 We find that this time constant is one of the most critical 440
 parameters in the model, and that the slow time scale of this 441
 gating for small stimulation amplitude is the main factor 442
 causing facilitation in the proctolin conditions at low pre- 443
 synaptic stimulation amplitude. 444

445 Equations describing MI channel gating yield standard
 first-order activation kinetics: 446

$$\begin{aligned} \frac{dx}{dt} &= k^+(1-x) - k^-x = (k^+ + k^-) \left(\frac{k^+}{k^+ + k^-} - x \right) \\ &= \frac{x_\infty(V) - x}{\tau_\infty(V)} \end{aligned} \quad (9)$$

447 where x is the fraction of I_{MI} channels in forms C^1 and O . 448
 The Ca^{2+} influx through the MI channel is then given by 449
 450

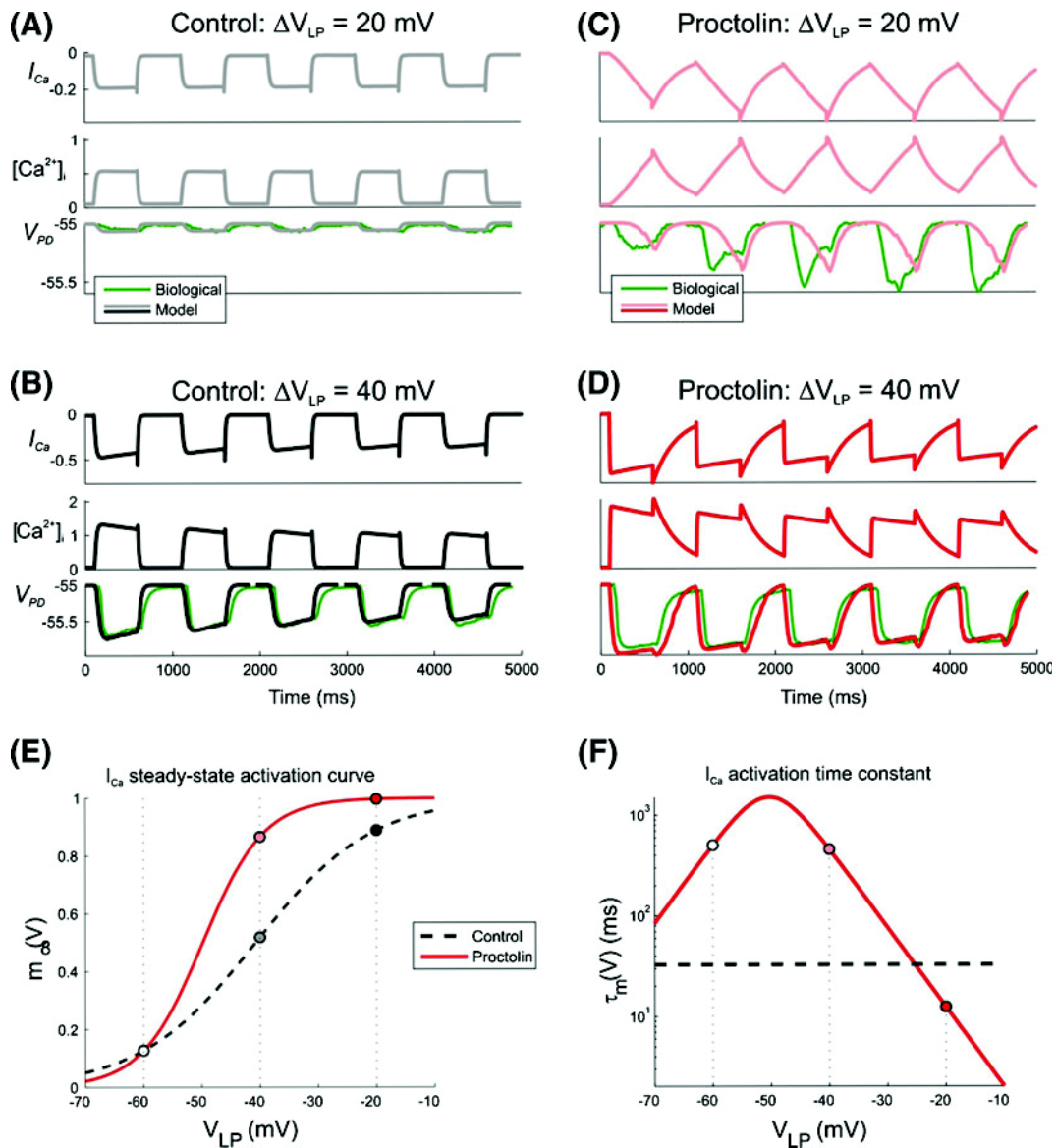


Fig. 3 Effects of proctolin in model I on LP to PD synaptic transmission for a sample parameter set. The response of the model with the parameter set shown in red in Fig. 2(a) to trains of low- and high-amplitude pulses in control and proctolin is compared to a biological recording (green traces) of the IPSPs in the PD neuron in one experiment different than the one shown in Fig. 1(a). (a) The model response to low-amplitude (20 mV) $K_{Ca} = 1.17\mu M$, $\bar{g}_{syn} = 6.06nS/\mu M^4$, pulses in the presynaptic LP neuron in control shows no significant IPSP in the PD neuron. (b) The model response to high-amplitude (40 mV) presynaptic pulses shows synaptic depression in control. (c) A switch to synaptic facilitation by proctolin. Proctolin changes the steady-state activation and time constant of I_{Ca} which leads to a

gradually-increasing IPSP in the PD neuron due to the gradual increase of $[Ca^{2+}]_i$ in presynaptic terminal. (d) Although Ca^{2+} entry is enhanced with high-amplitude voltage pulses in proctolin, a change in the activation kinetics results in synaptic depression. (e) Steady-state activation of I_{Ca} in control and in proctolin. Proctolin shifts the activation curve to the left and changes its slope, which leads to enhanced synaptic strength of the LP to PD synapse in the biological range. (f) Activation time constant of I_{Ca} in control and in proctolin. Parameter values are: $\bar{g}_{Ca} = 8.09nS$, $g_m = 0.416\mu S$, $\tau_h = 2.08s$, $\tau_{Ca} = 18.4ms$, $\tau_m^c = 32.8ms$, $V_h = 19.1mV$, $S_h = 4.56mV$, $V_m = 40.8mV$, $S_m = 10mV$, $V_m^p = 49.8mV$, $S_m^p = 5.27mV$, $A_\tau^c = 1.51s$, $V_\tau^p = 50.3mV$, $S_\tau^p = 5.51mV$

$$I_{MI-Ca} = \bar{g}_{MI}x(V - V_{Ca}) \quad (10)$$

453 where $V_{Ca} = 100mV$ is the equilibrium potential of Ca^{2+} , and
454 \bar{g}_{MI} is the maximal conductance of the MI channel.

455 In this model there are two sources of Ca^{2+} influx, the
456 principal Ca^{2+} channels and the MI channels, so the calcium

concentration $[Ca^{2+}]_i$ in the presynaptic LP neuron is 457

$$\frac{d[Ca^{2+}]_i}{dt} = -\frac{[Ca^{2+}]_i}{\tau_{Ca}} - \lambda I_{Ca} - \lambda I_{MI-Ca} \quad (11)$$

where τ_{Ca} and λ are same as in model I. In contrast to model 458
I, the activation time constant τ_m of I_{Ca} is fixed to the same 460

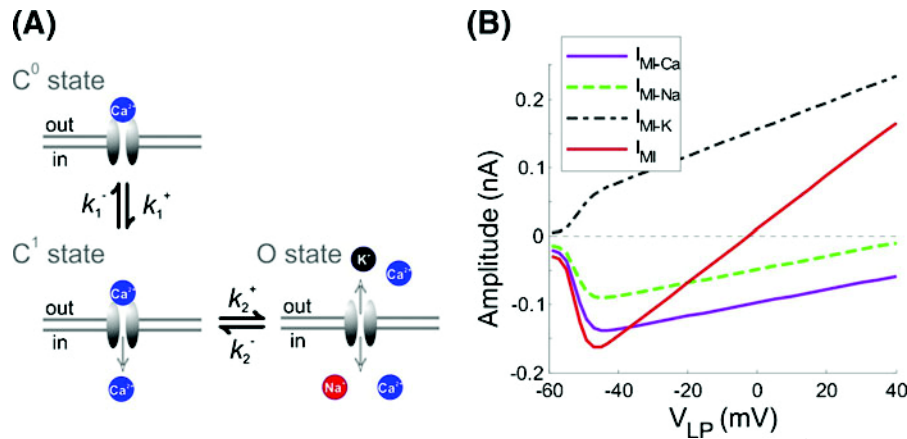


Fig. 4 Modulatory I_{MI} channel gating in model II. (a) Schematic diagram of transitions between states C^0 , C^1 , O of the MI channel. Channel state C^0 has the highest affinity for Ca^{2+} and the channel pore is completely blocked by Ca^{2+} , leading to zero cation permeability. Channel state C^1 has lower but significant Ca^{2+} affinity, allowing some Ca^{2+} ions to pass through upon their binding to the channel pore selectivity site but with no permeability to Na^+ and K^+ . Channel state O has very low Ca^{2+} affinity, allowing unrestricted flow of Na^+ and K^+ .

(b) The maximum amplitude of Ca^{2+} ($I_{MI-Ca}(nA)$; magenta curve), Na^+ ($I_{MI-Na}(nA)$; green dashed curve), K^+ ($I_{MI-K}(nA)$; black dash-dotted curve), and the total MI current ($I_{MI}(nA)$; red curve) influx through the modulatory channel I_{MI} when the presynaptic cell is depolarized from the resting potential $-60 mV$. The influx is measured in response to the last pulse of the five pulses train. The maximum influx of Ca^{2+} and I_{MI} occurs at around $-40 mV$

461 value as in control state (c.f. Eq. (7) in model I). Therefore,
 462 in this model the principal Ca^{2+} channels are unaffected by
 463 proctolin and proctolin targets MI channels only, which play
 464 the main role in the proctolin-induced change of synaptic
 465 dynamics.

466 To examine whether our model of the MI channel is con-
 467 sistent with previously published results on the voltage-
 468 dependence of this channel, we modeled the currents due to
 469 the flux of other cations (Na^+ and K^+) through this channel as
 470 well. The total current through the channel would be the sum
 471 of the currents due to Na^+ , K^+ and Ca^{2+} . Figure 4(b) shows the
 472 maximum amplitude of I_{MI} due to Ca^{2+} (I_{MI-Ca} , magenta),
 473 Na^+ (I_{MI-Na} , green), K^+ (I_{MI-K} , black), as well as the total MI
 474 current (I_{MI} , red) as a function of the holding membrane
 475 potential. The maximum amplitude of each component of
 476 I_{MI} depends on the stimulation voltage; the total current rea-
 477 ches its maximum influx at around $-40 mV$, consistent with
 478 previously reported experimental results (Golowasch and
 479 Marder 1992). Note that this figure shows the steady state
 480 maximum amplitude of current flux produced by voltage
 481 pulses and does not use the assumption that the C^1 and O
 482 states are collapsed into one state.

483 The proposed MI channel model assumes that the slow
 484 changes in the conformational state of the MI channel gener-
 485 ate a gradual increase of Ca^{2+} influx into the presynaptic
 486 terminal through the MI channels in the C^1 state (Fig. 4(a)),
 487 which is qualitatively similar to the increase in Ca^{2+} obtained
 488 in the model I. The synaptic response caused by I_{MI} gating
 489 exhibits facilitation if the Ca^{2+} influx through modulatory
 490 channels constitutes a considerable fraction of the total
 491 voltage-gated Ca^{2+} influx. This assumption leads to experi-
 492 mentally testable predictions, as described in the discussion.

As with model I, to obtain proper fits for the actions of
 proctolin in model II, we used an optimization algorithm to
 fit the synaptic output in both control and proctolin condi-
 tions and with presynaptic amplitudes of 20 mV and 40 mV.
 A total of 198 randomly-seeded parameter sets were opti-
 mized and the overall range of parameter distributions for
 the fits is shown in Fig. 5. The parameters that were rela-
 tively tightly constrained included (as in model I) the mid-
 point of the Ca^{2+} current activation curve and K_{Ca} , the
 calcium affinity of neurotransmitter release (Fig. 5(a)).

As in model I, there was no global relationship among
 parameter sets that provided best fit values in this model
 (two examples shown in Fig. 5(a)). Also, as in model I, few
 parameter pairs showed strong pair-wise correlations. The
 negative correlations included the midpoint and slope of the
 Ca^{2+} current activation curve and the midpoint and slope of
 the MI current activation (Fig. 5(b)), indicating that the shift
 of the midpoint of the activation curve to the right was
 correlated with an increase in its slope.

Figure 6 shows the effect of proctolin in model II for one
 optimized parameter set, tested at two different amplitudes of
 presynaptic LP neuron stimulation. For any presynaptic pulse
 amplitude, $[Ca^{2+}]_i$ was higher in proctolin than in control state
 due to Ca^{2+} entry through the MI channels (I_{MI-Ca}) whereas
 Ca^{2+} entry through Ca^{2+} channels (I_{Ca}) remained unmodulated
 and unchanged. For high-amplitude (40 mV) presynaptic
 stimuli, the dominant part of Ca^{2+} influx was through the
 principal Ca^{2+} channels and therefore synaptic response still
 showed depression, as in the control state, despite the small
 gradual increase in I_{MI-Ca} . However, for the low-amplitude
 (20 mV) presynaptic stimulation, I_{MI-Ca} had more influence
 on total Ca^{2+} entry, resulting in the gradual increase of $[Ca^{2+}]_i$

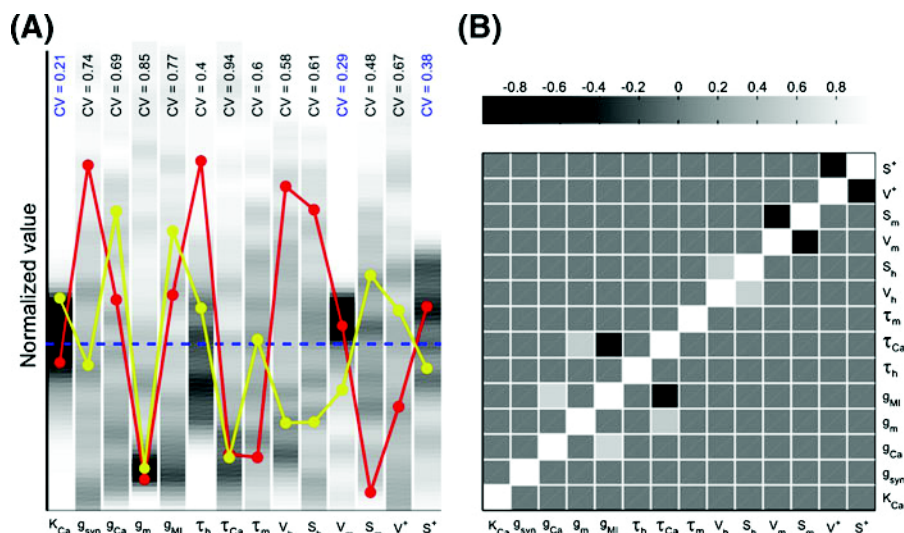


Fig. 5 Optimized parameter set $K_{Ca} = 1.9\mu M$, $\bar{g}_{syn} = 5.1 nS/\mu M^4$, $\bar{g}_{Ca} = 29.4nS$, τ_s showing the modulation of MI channels by proctolin in model II. A total of 198 randomly-seeded parameter sets were optimized for model II to fit the experimental recording of the synaptic outputs in control and proctolin for two different presynaptic voltage amplitudes (see Methods). (a) The distribution of parameter values for 14 of 15 parameters in model II. (In all parameter sets k^- converged to a value very close to the lower limit of $0.1 s^{-1}$ during optimization, and is not shown.) The value of each parameter was normalized to the mean value of its distribution (dashed blue line) for comparison; these mean values are: $g_m = 34.8nS$, $g_{MI} = 2.06nS$, $\tau_h = 587ms$, $\tau_{Ca} = 26.5ms$, $\tau_m = 41.8ms$, $V_h = 61.6mV$, $S_h = 27.7mV$, $V_m = 36.8mV$, $S_m = 14.1mV$, $V^+ = 14.7mV$, $S^+ = 3.61mV$. Two parameter sets are also shown for comparison (red and yellow), demonstrating that good fits to the data did not require a consistent relationship among all parameters. Three out of the 14 parameters were relatively tightly constrained by the optimization technique (coefficient of variation < 0.4 shown in blue). (b) Pair-wise correlations among the best-fit parameters indicate that few parameter pairs showed any significant ($R > 0.5$) co-variation

525 in presynaptic terminal and the change of synaptic dynamics
 526 from depression to facilitation. Note that, in this model, accu-
 527 mulation of $[Ca^{2+}]_i$ over multiple pulses depended on the slow
 528 I_{MI-Ca} deactivation time constant (Fig. 6(f)) or, equivalently,
 529 on a small value of k^- . Although we did not allow the value of
 530 this rate constant to go below $0.1 s^{-1}$ in our simulations, in all
 531 parameter sets k^- converged to a value very close to this lower
 532 limit during optimization (and hence it is not shown in Fig. 5
 533 (a)).

534 **4 Discussion**

535 Neuromodulators can change synaptic strength by modifying
 536 either presynaptic transmitter release or the postsynaptic re-
 537 ceptor response (Johnson and Harris-Warrick 1997). Our pre-
 538 vious experimental findings indicate that the enhancement of
 539 the LP to PD synapse by proctolin is correlated with an
 540 increase in a presynaptic inward current (Zhao et al. 2011).
 541 This inward current is blocked by Mn^{2+} , suggesting that it is a
 542 Ca^{2+} current, and its accumulation over multiple presynaptic
 543 voltage pulses is strongly correlated with the facilitation of the
 544 postsynaptic IPSP. The current modeling study therefore fo-
 545 cused only on presynaptic effects in accordance with this
 546 result and other experimental evidence (Zhao et al. 2011).

547 To explore the mechanisms underlying the effects of proctolin
 548 on the short-term dynamics of the LP to PD synapse, we
 549 used computational modeling to examine two alternative

hypotheses to find the most parsimonious explanation for
 the proctolin-mediated modulation of this synapse. Both mod-
 els assume that the observed changes in synaptic properties
 are caused by changes in intracellular Ca^{2+} dynamics in the
 presynaptic LP neuron. Each of the two models reproduces
 facilitation at low presynaptic voltages, explaining it by the
 gradual increase in Ca^{2+} concentration in the presynaptic
 terminal due to the changes of Ca^{2+} influx from pulse to pulse
 through I_{Ca} and I_{MI} channels, respectively. Additionally, in
 both models it is important for these channels to be close to the
 presynaptic sites of transmitter release for the mechanisms
 described to work.

Model I is based on the ideas put forth in our earlier
 modeling study in which we examined the potential for
 intracellular Ca^{2+} ion accumulation for producing the syn-
 aptic facilitation observed in the presence of proctolin (Zhou
 et al. 2007). In that study, we described the switch from
 depression to facilitation using two low-threshold and one
 high-threshold Ca^{2+} currents which, as shown in the current
 study, can be accomplished with a single Ca^{2+} current. The
 simplification of the model in the current study facilitated a
 direct comparison of the mechanisms underlying the neuro-
 modulation of synaptic plasticity.

It is known that the neuromodulator dopamine exerts its
 action partially by modulating calcium currents in pyloric
 neurons (Johnson et al. 2003). Enhancement or reduction of
 I_{Ca} is consistent with dopamine-induced synaptic strength
 changes. Similarly, one possible explanation of proctolin-

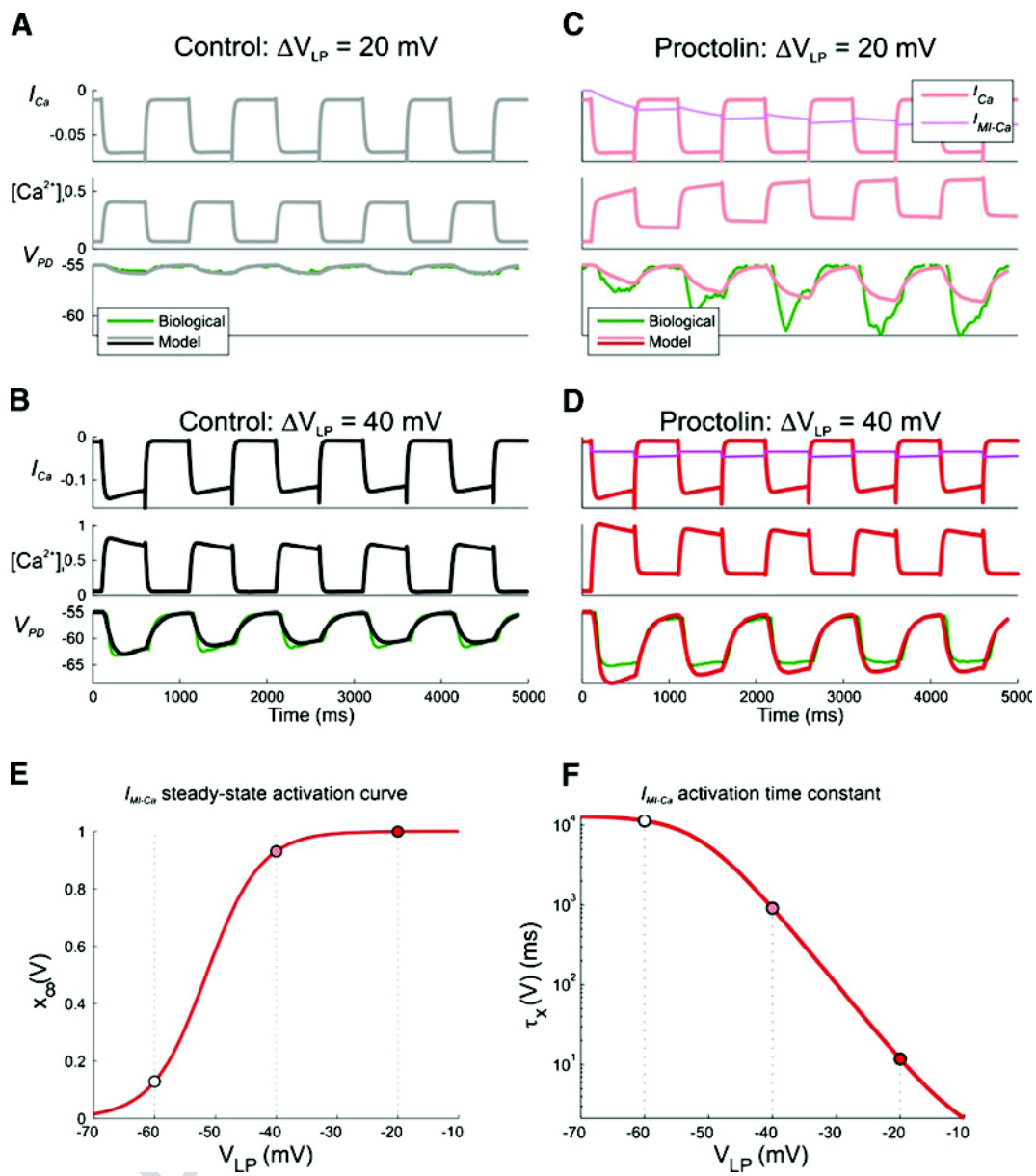


Fig. 6 Effects of proctolin in model II on LP to PD synaptic transmission for a sample parameter set. The response of the model with the parameter set shown in red in Fig. 5(a) to trains of low- and high-amplitude pulses in control and proctolin is compared to a biological recording (green traces) of the IPSPs in the PD neuron in one experiment (same as Fig. 3). (a) The model response to low-amplitude (20 mV) pulses in the presynaptic LP neuron in control shows no significant IPSP in the PD neuron. (b) The model response to high-amplitude (40 mV) presynaptic pulses shows synaptic depression in control. (c) A switch to synaptic facilitation by proctolin. A gradual increase of $[Ca^{2+}]_i$ in presynaptic terminal due to the Ca^{2+} entry

through MI channels allows for observed facilitation. (d) Although the increase in $[Ca^{2+}]_i$ due to the MI channels is still present, the dominant effect on $[Ca^{2+}]_i$ is due to I_{Ca} , resulting in depression as in control. (e) Steady-state activation of I_{Ca} in control and in proctolin. Proctolin shifts the activation curve to the left and changes its slope, which leads to enhanced synaptic strength of the LP to PD synapse in the biological range. (f) Activation time constant of I_{Ca} in control and in proctolin. Parameter values are: $K_{Ca} = 1.7\mu M$, $\bar{g}_{syn} = 10nS/\mu M^4$, $\bar{g}_{Ca} = 37.4nS$, $g_m = 7.4nS$, $g_{MI} = 2.68nS$, $\tau_h = 1.23s$, $\tau_{Ca} = 9.57ms$, $\tau_m = 14.3ms$, $V_h = 120mV$, $S_h = 49.8mV$, $V_m = 41.1mV$, $S_m = 1.91mV$, $V^+ = 9.45mV$, $S^+ = 4.44mV$

578 induced synaptic strength changes is via modulation of
 579 presynaptic I_{Ca} , which is captured by the Ca^{2+}
 580 model (model I). The modulatory channel model (model
 581 II) is dependent on Ca^{2+} influx through both a Ca^{2+}
 582 and a proctolin-activated non-specific cation channel.
 583 Results of Stout et al. (1996) suggest that there is a

glutamate-induced Mg^{2+} influx through the NMDA receptor
 ion channel. The proctolin-modulated MI channels are similar
 to NMDA receptor channels in that they are believed to
 be partially blocked by Ca^{2+} at low membrane potentials
 (Golowasch and Marder 1992). This led us to our second
 hypothesis that the modulation of the LP to PD synapse may

590 be caused by the voltage-sensitive changes in Ca^{2+} -perme- 643
591 ability of the MI channels which has some recent experi- 644
Q4 592 mental support (Gray and Golowasch 2011). 645

593 Although both models successfully reproduce the observed 646
594 dynamic changes in the LP to PD synapse by proctolin, the 647
595 two models predict different voltage dependence of the total 648
596 steady-state Ca^{2+} current, which can be verified experimen- 649
597 tally. In particular, experiments that combine Ca^{2+} imaging 650
598 with Cd^{2+} block (which, unlike Mn^{2+} , does not affect I_{MI} 651
599 (Golowasch and Marder 1992)) of the principal voltage- 652
600 dependent calcium channels may reveal changes in the Ca^{2+} 653
601 permeability of the modulatory channels. 654

602 Note that the two proposed models make distinct predic- 655
603 tions for the interaction between intrinsic and synaptic prop- 656
604 erties that determines neuronal network activity. Model I 657
605 may only be relevant for the LP to PD synapse, because 658
606 proctolin may only modulate local Ca^{2+} channels at this 659
607 particular synapse, and may have no effect on other synap- 660
608 ses in pyloric network or even other synapses from the same 661
609 presynaptic LP neuron, for example the LP to PY synapse 662
610 (Mamiya and Nadim 2005). Further, if other neuromodula- 663
611 tors do not modulate presynaptic Ca^{2+} channels at this 664
612 synapse, then the described results are specific to the effect 665
613 of proctolin on the LP to PD synapse only. On the other 666
614 hand, model II is likely to be applicable not only to the LP- 667
615 PD synapse but also to other synapses in the pyloric net- 668
616 work, because proctolin activates I_{MI} in other neurons of the 669
617 same circuit. Moreover, other neuromodulators such as 670
618 RPCH and CCAP are also known to activate MI channels 671
619 (Swensen and Marder 2000). If model II is valid, a similar 672
620 modulatory effect on synaptic dynamics may be observed 673
621 throughout the network and may be subserved by a variety 674
622 of modulatory substances. 675

623 The parameter values in the two models were set by opti- 676
624 mizing the fit between model and data, which accomplishes 677
625 several goals. First, it leads to a more thorough parameter- 678
626 sensitivity analysis, allowing a more thorough exploration of 679
627 parameter sets that are consistent with experimental observa- 680
628 tions. Preceding the parameter optimization with random pa- 681
629 rameter search significantly improves such sampling of 682
630 parameter space. More importantly, the optimization allows 683
631 one to establish or validate the mechanism by which elements 684
632 of a chosen model capture the observed features of data, in this 685
633 case depression or facilitation under control conditions or in 686
634 the presence of proctolin. For instance, we hypothesized that 687
635 model I would reproduce the observed facilitation in proctolin 688
636 for low-amplitude stimulation if proctolin were to shift the 689
637 Ca^{2+} current activation to more negative potentials, and si- 690
638 multaneously change its activation time constant. This was 691
639 substantiated by the parameter optimization, since Fig. 2(a) 692
640 shows that parameters that were most tightly constrained by 693
641 data fit optimization correspond to the I_{Ca} half-activation 694
642 potentials in control and proctolin, V_m and V_m^p , as well as the 695

control potential of activation time constant in proctolin, V_p^p . 643
Similarly, in model II we found that optimization always led to 644
a decrease in the value of k to its allowed bottom bound of 645
 0.1 s^{-1} , indicating that the only mechanism by which model II 646
can explain facilitation in proctolin for low-amplitude stimu- 647
lation is the gradual growth of the $I_{\text{MI-Ca}}$ current caused by its 648
slow de-activation. This conclusion was further verified by 649
examining the time traces of simulated PD potential and $I_{\text{MI-Ca}}$ 650
for all optimized parameter sets. 651

652 Short-term dynamics of synaptic transmission have been 653
654 modeled in a number of synapses subserving a variety 655
656 of activities (Abbott et al. 1997; Hermann et al. 2009; 657
658 Gundlfinger et al. 2007; Markram and Tsodyks 1996; 659
660 Tsodyks et al. 1998). The basic feature of most of these 661
662 models is that vesicle release from a readily releasable pool 663
664 is generally considered crucial in explaining short-term 665
666 plasticity. The classic presynaptic vesicle depletion model 667
668 is often used to explain depression dynamics (Thies 1965; 669
670 von Gersdorff et al. 1997; Wu and Betz 1998) whereas 671
672 calcium-dependent transmitter release is usually invoked to 673
674 model facilitation (Bertram et al. 1996; Matveev et al. 675
676 2006). Some studies at a large mammalian central synapse, 677
678 the calyx of Held in the rat medial nucleus of the trapezoid 679
680 body, indicate that regulation of voltage-gated Ca^{2+} chan- 681
682 nels is important in mediating short-term plasticity. For 683
684 instance, inactivation of presynaptic Ca^{2+} currents is a major 685
686 mechanism underlying short-term depression for a wide 687
688 range of stimulation conditions (Xu and Wu 2005) whereas 689
690 the facilitation of I_{Ca} mediated in a Ca^{2+} -dependent manner 691
692 (Borst and Sakmann 1998; Cuttle et al. 1998; Tsujimoto et 693
694 al. 2002) contributes significantly to short-term facilitation 695

696 The mathematical models of neuromodulation of short- 697
698 term synaptic dynamics developed in this paper are minimal 699
700 in the sense that the presynaptic I_{Ca} is incorporated into a 701
702 combined pre- and postsynaptic model using a minimal set 703
704 of assumptions consistent with experimental findings. The 705
706 advantage of this minimal approach is that the resulting 707
708 models can be more easily tested with further experimenta- 709
710 tion. The small number of equations makes these models 711
712 amenable to network simulations and the minimal imple- 713
714 mentation highlights those features of the presynaptic Ca^{2+} 715
716 influx through Ca^{2+} or modulatory channels that play an 717
718 important role in synaptic dynamics. Furthermore, our study 719
720 demonstrates the plausibility of the hypothesis that neuro- 721
722 modulation of non-specific cation channels other than the 723
724 principal presynaptic Ca^{2+} channels may influence synaptic 725
726 release and therefore postsynaptic potentials. We note that 727
728 non-specific ion channels show permeability to Ca^{2+} ions in 729
730 a variety of systems, and therefore this finding has broader 731
732 implications for potential mechanisms of neuromodulation 733
734 of synaptic dynamics. 735

697 **Acknowledgements** This work was supported by the National Sci-
 698 ence Foundation grant DMS-0817703 (VM) and the National Institute
 699 of Mental Health grant MH060605 (FN).

700 **References**

702 Abbott, L. F., Varela, J. A., Sen, K., & Nelson, S. B. (1997). Synaptic
 703 depression and cortical gain control. *Science*, 275(5297), 220–224.
 704 Ayali, A., Johnson, B. R., & Harris-Warrick, R. M. (1998). Dopamine
 705 modulates graded and spike-evoked synaptic inhibition independ-
 706 dently at single synapses in pyloric network of lobster. *Journal of*
 707 *Neurophysiology*, 79(4), 2063–2069.
 708 Babich, O., Matveev, V., Harris, A. L., & Shirokov, R. (2007). Ca²⁺-
 709 dependent inactivation of CaV1.2 channels prevents Gd³⁺ block:
 710 does Ca²⁺ block the pore of inactivated channels? *Journal of*
 711 *General Physiology*, 129(6), 477–483.
 712 Bardoni, R., Torsney, C., Tong, C. K., Prandini, M., & MacDermott, A.
 713 B. (2004). Presynaptic NMDA receptors modulate glutamate
 714 release from primary sensory neurons in rat spinal cord dorsal
 715 horn. *Journal of Neuroscience*, 24(11), 2774–2781.
 716 Barriere, G., Tartas, M., Cazalets, J. R., & Bertrand, S. S. (2008).
 717 Interplay between neuromodulator-induced switching of short-
 718 term plasticity at sensorimotor synapses in the neonatal rat spinal
 719 cord. *The Journal of Physiology*, 586(7), 1903–1920.
 720 Berretta, N., & Jones, R. S. (1996). Tonic facilitation of glutamate
 721 release by presynaptic N-methyl-D-aspartate autoreceptors in the
 722 entorhinal cortex. *Neuroscience*, 75(2), 339–344.
 723 Bertram, R., Sherman, A., & Stanley, E. F. (1996). Single-domain/
 724 bound calcium hypothesis of transmitter release and facilitation.
 725 *Journal of Neurophysiology*, 75(5), 1919–1931.
 726 Bertram, R., Swanson, J., Yousef, M., Feng, Z. P., & Zamponi, G. W.
 727 (2003). A minimal model for G protein-mediated synaptic facilita-
 728 tion and depression. *Journal of Neurophysiology*, 90(3), 1643–1653.
 729 Bieda, M. C., & Copenhagen, D. R. (2004). N-type and L-type calcium
 730 channels mediate glycinergic synaptic inputs to retinal ganglion
 731 cells of tiger salamanders. *Visual Neuroscience*, 21(4), 545–550.
 732 Borst, J. G., & Sakmann, B. (1998). Facilitation of presynaptic calcium
 733 currents in the rat brainstem. *The Journal of Physiology*, 513(Pt
 734 1), 149–155.
 735 Buchholtz, F., Golowasch, J., Epstein, I. R., & Marder, E. (1992).
 736 Mathematical model of an identified stomatogastric ganglion
 737 neuron. *Journal of Neurophysiology*, 67(2), 332–340.
 738 Chance, F. S., Nelson, S. B., & Abbott, L. F. (1998). Synaptic depres-
 739 sion and the temporal response characteristics of V1 cells. *Journal*
 740 *of Neuroscience*, 18(12), 4785–4799.
 741 Cuttle, M. F., Tsujimoto, T., Forsythe, I. D., & Takahashi, T. (1998).
 742 Facilitation of the presynaptic calcium current at an auditory
 743 synapse in rat brainstem. *The Journal of Physiology*, 512(Pt 3),
 744 723–729.
 745 Dittman, J. S., Kreitzer, A. C., & Regehr, W. G. (2000). Interplay
 746 between facilitation, depression, and residual calcium at three
 747 presynaptic terminals. *Journal of Neuroscience*, 20(4), 1374–
 748 1385.
 749 Fossier, P., Tauc, L., & Baux, G. (1999). Calcium transients and
 750 neurotransmitter release at an identified synapse. *Trends in Neuro-*
 751 *sciences*, 22(4), 161–166.
 752 Galaneta, M., & Hestrin, S. (1998). Frequency-dependent synaptic
 753 depression and the balance of excitation and inhibition in the
 754 neocortex. *Nature Neuroscience*, 1(7), 587–594.
 755 Golowasch, J., & Marder, E. (1992). Proctolin activates an inward
 756 current whose voltage dependence is modified by extracellular
 757 Ca²⁺. *Journal of Neuroscience*, 12(3), 810–817.
 Q758 Gray, M. L., & Golowasch, J. Intracellular signaling of peptidergic
 759 neuromodulatory input to the pyloric network in the stomatogastric

ganglion of *Cancer borealis*. In *Soc Neurosci Abst, 2011* (Vol. 37, 760
 Vol. 707.04) 761
 Gundlfinger, A., Leibold, C., Gebert, K., Moisel, M., Schmitz, D., & 762
 Kemper, R. (2007). Differential modulation of short-term synaptic 763
 dynamics by long-term potentiation at mouse hippocampal mossy 764
 fibre synapses. *The Journal of Physiology*, 585(Pt 3), 853–865. 765
 Hermann, J., Grothe, B., & Klug, A. (2009). Modeling short-term 766
 synaptic plasticity at the calyx of held using in vivo-like stimula- 767
 tion patterns. *Journal of Neurophysiology*, 101(1), 20–30. 768
 Hige, T., Fujiyoshi, Y., & Takahashi, T. (2006). Neurosteroid pregnen- 769
 olone sulfate enhances glutamatergic synaptic transmission by 770
 facilitating presynaptic calcium currents at the calyx of Held of 771
 immature rats. *European Journal of Neuroscience*, 24(7), 1955– 772
 1966. 773
 Inchauspe, C. G., Martini, F. J., Forsythe, I. D., & Uchitel, O. D. 774
 (2004). Functional compensation of P/Q by N-type channels 775
 blocks short-term plasticity at the calyx of held presynaptic ter- 776
 minal. *Journal of Neuroscience*, 24(46), 10379–10383. 777
 Ishikawa, T., Kaneko, M., Shin, H. S., & Takahashi, T. (2005). Pre- 778
 synaptic N-type and P/Q-type Ca²⁺ channels mediating synaptic 779
 transmission at the calyx of Held of mice. *The Journal of Physi-* 780
ology, 568(Pt 1), 199–209. 781
 Johnson, B. R., Brown, J. M., Kvarta, M. D., Lu, J. Y., Schneider, L. 782
 R., Nadim, F., et al. (2011). Differential modulation of synaptic 783
 strength and timing regulate synaptic efficacy in a motor network. 784
Journal of Neurophysiology, 105(1), 293–304. 785
 Johnson, B. R., Kloppenburg, P., & Harris-Warrick, R. M. (2003). 786
 Dopamine modulation of calcium currents in pyloric neurons of 787
 the lobster stomatogastric ganglion. *Journal of Neurophysiology*, 788
 90(2), 631–643. 789
 Johnson, B. R., Schneider, L. R., Nadim, F., & Harris-Warrick, R. M. 790
 (2005). Dopamine modulation of phasing of activity in a rhythmic 791
 motor network: contribution of synaptic and intrinsic modulatory 792
 actions. *Journal of Neurophysiology*, 94(5), 3101–3111. 793
 Kreitzer, A. C., & Regehr, W. G. (2000). Modulation of transmission 794
 during trains at a cerebellar synapse. *Journal of Neuroscience*, 20 795
 (4), 1348–1357. 796
 Lagarias, J. C., Reeds, J. A., Wright, M. H., & Wright, P. E. 797
 (1998). Convergence properties of the Nelder-Mead simplex 798
 method in low dimensions. *SIAM Journal on Optimization*, 9 799
 (1), 112–147. 800
 Macleod, G. T., Hegstrom-Wojtowicz, M., Charlton, M. P., & Atwood, 801Q3
 H. L. (2002). Fast calcium signals in *Drosophila* motor neuron 802
 terminals. *Journal of Neurophysiology*, 88(5), 2659–2663. 803
 MacLeod, K. M., Horiuchi, T. K., & Carr, C. E. (2007). A role for 804
 short-term synaptic facilitation and depression in the processing 805
 of intensity information in the auditory brain stem. *Journal of* 806
Neurophysiology, 97(4), 2863–2874. 807
 Mamiya, A., Manor, Y., & Nadim, F. (2003). Short-term dynamics of a 808
 mixed chemical and electrical synapse in a rhythmic network. 809
Journal of Neuroscience, 23(29), 9557–9564. 810
 Mamiya, A., & Nadim, F. (2005). Target-specific short-term dynamics 811
 are important for the function of synapses in an oscillatory neural 812
 network. *Journal of Neurophysiology*, 94(4), 2590–2602. 813
 Manor, Y., Bose, A., Booth, V., & Nadim, F. (2003). Contribution of 814
 synaptic depression to phase maintenance in a model rhythmic 815
 network. *Journal of Neurophysiology*, 90(5), 3513–3528. 816
 Manor, Y., Nadim, F., Abbott, L. F., & Marder, E. (1997). Temporal 817
 dynamics of graded synaptic transmission in the lobster stomato- 818
 gastric ganglion. *Journal of Neuroscience*, 17(14), 5610–5621. 819
 Marder, E., & Bucher, D. (2007). Understanding circuit dynamics 820
 using the stomatogastric nervous system of lobsters and crabs. 821
Annual Review of Physiology, 69, 291–316. 822
 Markram, H., & Tsodyks, M. (1996). Redistribution of synaptic effi- 823
 cacy between neocortical pyramidal neurons. *Nature*, 382(6594), 824
 807–810. 825

- 826 Matveev, V., Bertram, R., & Sherman, A. (2006). Residual bound Ca²⁺
827 can account for the effects of Ca²⁺ buffers on synaptic facilitation.
828 *Journal of Neurophysiology*, *96*, 3389–3397.
- 829 Nadim, F., Booth, V., Bose, A., & Manor, Y. (2003). Short-term
830 synaptic dynamics promote phase maintenance in multi-phasic
831 rhythms. *Neurocomputing*, *52–4*, 79–87.
- 832 Olcese, R. (2007). And yet it moves: conformational States of the Ca²⁺
833 channel pore. *Journal of General Physiology*, *129*(6), 457–459.
- 834 Pan, B., & Zucker, R. S. (2009). A general model of synaptic trans-
835 mission and short-term plasticity. *Neuron*, *62*(4), 539–554.
- 836 Reyes, A., Lujan, R., Rozov, A., Burnashev, N., Somogyi, P., &
837 Sakmann, B. (1998). Target-cell-specific facilitation and depres-
838 sion in neocortical circuits. *Nature Neuroscience*, *1*(4), 279–285.
- 839 Rose, G., & Fortune, E. (1999). Frequency-dependent PSP depression
840 contributes to low-pass temporal filtering in *Eigenmannia*. *Jour-
841 nal of Neuroscience*, *19*(17), 7629–7639.
- 842 Schneggenburger, R., & Neher, E. (2005). Presynaptic calcium and
843 control of vesicle fusion. *Current Opinion in Neurobiology*, *15*(3),
844 266–274.
- 845 Stout, A. K., Li-Smerin, Y., Johnson, J. W., & Reynolds, I. J. (1996).
846 Mechanisms of glutamate-stimulated Mg²⁺ influx and subse-
847 quent Mg²⁺ efflux in rat forebrain neurones in culture. *The
848 Journal of Physiology*, *492*(Pt 3), 641–657.
- 849 Swensen, A. M., & Marder, E. (2000). Multiple peptides converge to
850 activate the same voltage-dependent current in a central pattern-
851 generating circuit. *Journal of Neuroscience*, *20*(18), 6752–6759.
- 852 Swensen, A. M., & Marder, E. (2001). Modulators with convergent
853 cellular actions elicit distinct circuit outputs. *Journal of Neurosci-
854 ence*, *21*(11), 4050–4058.
- 855 Thies, R. E. (1965). Neuromuscular depression and the apparent de-
856 pletion of transmitter in mammalian muscle. *Journal of Neuro-
857 physiology*, *28*, 428–442.
- 858 Thirumalai, V., Prinz, A. A., Johnson, C. D., & Marder, E. (2006). Red
859 pigment concentrating hormone strongly enhances the strength of
860 the feedback to the pyloric rhythm oscillator but has little effect on
861 pyloric rhythm period. *Journal of Neurophysiology*, *95*(3), 1762–
862 1770.
- 863 Tsodyks, M., Pawelzik, K., & Markram, H. (1998). Neural networks
864 with dynamic synapses. *Neural Computation*, *10*(4), 821–835.
- 865 Tsodyks, M. V., & Markram, H. (1997). The neural code between
866 neocortical pyramidal neurons depends on neurotransmitter
908 release probability. *Proceedings of the National Academy of Sci-
ences of the United States of America*, *94*(2), 719–723.
- Tsujimoto, T., Jeromin, A., Saitoh, N., Roder, J. C., & Takahashi, T. (2002). Neuronal calcium sensor 1 and activity-dependent facilitation of P/Q-type calcium currents at presynaptic nerve terminals. *Science*, *295*(5563), 2276–2279.
- Verhoog, M. B., & Mansvelder, H. D. (2011). Presynaptic ionotropic receptors controlling and modulating the rules for spike timing-dependent plasticity. *Neural Plasticity*, *2011*, 870763.
- von Gersdorff, H., Schneggenburger, R., Weis, S., & Neher, E. (1997). Presynaptic depression at a calyx synapse: the small contribution of metabotropic glutamate receptors. *Journal of Neuroscience*, *17*(21), 8137–8146.
- Wang, S. J., Wang, K. Y., Wang, W. C., & Sihra, T. S. (2006). Unexpected inhibitory regulation of glutamate release from rat cerebrocortical nerve terminals by presynaptic 5-hydroxytryptamine-2A receptors. *Journal of Neuroscience Research*, *84*(7), 1528–1542.
- Wu, L. G., & Betz, W. J. (1998). Kinetics of synaptic depression and vesicle recycling after tetanic stimulation of frog motor nerve terminals. *Biophysical Journal*, *74*(6), 3003–3009.
- Wu, L. G., & Saggau, P. (1997). Presynaptic inhibition of elicited neurotransmitter release. *Trends in Neurosciences*, *20*(5), 204–212.
- Xu, J., He, L., & Wu, L. G. (2007). Role of Ca(2+) channels in short-term synaptic plasticity. *Current Opinion in Neurobiology*, *17*(3), 352–359.
- Xu, J., & Wu, L. G. (2005). The decrease in the presynaptic calcium current is a major cause of short-term depression at a calyx-type synapse. *Neuron*, *46*(4), 633–645.
- Yue, D. T., Backx, P. H., & Imredy, J. P. (1990). Calcium-sensitive inactivation in the gating of single calcium channels. *Science*, *250*(4988), 1735–1738.
- Zhao, S., Sheibanie, A. F., Oh, M., Rabbah, P., & Nadim, F. (2011). Peptide neuromodulation of synaptic dynamics in an oscillatory network. *Journal of Neuroscience*, *31*(39), 13991–14004.
- Zhou, L., Zhao, S., & Nadim, F. (2007). Neuromodulation of short-term synaptic dynamics examined in a mechanistic model based on kinetics of calcium currents. *Neurocomputing*, *70*(10–12), 2050–2054.
- Zucker, R. S., & Regehr, W. G. (2002). Short-term synaptic plasticity. *Annual Review of Physiology*, *64*, 355–405.